Intermolecular interaction in the CH_3^+–He ionic complex revealed by *ab initio* calculations and infrared photodissociation spectroscopy

Rouslan V. Olkhov, Sergey A. Nizkorodov,[a] and Otto Dopfer[b]
Institut für Physikalische Chemie, Universität Basel, Klingelbergstrasse 80, CH-4056 Basel, Switzerland

(Received 15 January 1999; accepted 23 February 1999)

The infrared photodissociation spectrum of the degenerate asymmetric CH stretch (ν_3) vibration of the CH_3^+–He ionic complex has been recorded. The rotational structure and vibrational frequency of the observed transition are consistent with a π-bonded C_{3v} cluster geometry where the He ligand is attached to the $2p_z$ orbital of the central C atom of CH_3^+. The intermolecular bond in the ground vibrational state is characterized by an averaged intermolecular separation of $R_{cm}=2.18$ Å. The origin of the ν_3 vibration of the complex is slightly blue shifted (7 cm^{-1}) compared to the monomer frequency, indicating that vibrational excitation is accompanied by a slight destabilization of the intermolecular bond. *Ab initio* calculations at the MP2/aug-cc-pVTZ# level of theory confirm that the π-bonded configuration corresponds to the global minimum structure of the complex ($D_e=707\,cm^{-1}$, $R_e=1.834$ Å). The calculated intermolecular potential energy surface of this ''disk-and-ball'' ionic complex reveals substantial angular-radial couplings in the region of the global minimum, which account for the large discrepancy between vibrationally averaged and calculated equilibrium intermolecular separations, $R_{cm}-R_e=0.35$ Å. © *1999 American Institute of Physics.* [S0021-9606(99)02319-3]

I. INTRODUCTION

Intermolecular interactions in ionic complexes bridge the gap between weak van der Waals forces acting in neutral clusters and strong chemical bonds of molecular species. Despite their importance in many areas of physical chemistry (e.g., ion–molecule reactions, plasma physics, solvation processes)[1–3] and biology (e.g., structure of biomolecules, transmembrane ion transport),[4] ion-neutral interactions are spectroscopically not well characterized,[5,6] mainly owing to the difficulties involved in the production of high number densities of charged complexes. Recent progress in the development of sensitive experimental approaches that combine mass spectrometric with high resolution spectroscopic techniques can overcome this problem.[7–9] Our laboratory utilizes infrared photodissociation spectroscopy in a tandem mass spectrometer to study the intermolecular interaction in small ionic dimers. In addition, the microsolvation of ions has been investigated by monitoring the properties of size-selected clusters as a function of the surrounding neutral ligands.[10–13]

Rare gas (Rg) atoms have often been used as a structureless probe of the intermolecular interaction in ion-ligand complexes. Most of the previously studied ionic complexes are proton-bound dimers of the type A–H^+–Rg, where two bases A and Rg are held together by a linear proton bond.[10,13–18] Thermochemical and mass spectrometric studies demonstrated that the interaction strength in such dimers is correlated with the difference in the proton affinities (PA) of the two bases,[19,20] a conclusion that was confirmed by spectroscopic and *ab initio* studies.[13,21] In cases, where the PA of A is much higher than that of the Rg atom, the A–H^+–Rg complex can be viewed as an AH^+ molecular ion that is only weakly perturbed by the Rg ligand. Increasing the PA of A destabilizes the linear proton bond and other bonding sites around the AH^+ ion may become energetically more favorable for the Rg atom.[12,13] For example, a recent combined spectroscopic and theoretical study on CH_3^+–Ar_n complexes ($n=1-8$) revealed that, owing to the high PA of CH_2, the proton-bound planar structure of the CH_3^+–Ar dimer is significantly less stable than the ''π-bound'' configuration, where the Ar atom is attached to the $2p_z$ orbital of the carbon atom (C_{3v} symmetry) and therefore closer to the center of the positive charge distribution.[12] *Ab initio* calculations indicated that the high binding energy of this π-bound structure (≈0.5 eV) is partly due to a partial charge transfer from Ar into the vacant electrophilic $2p_z$ orbital of carbon.[12,22] The formation of this strong charge-transfer bond is accompanied by a massive deformation of the CH_3^+ geometry; it changes from a planar D_{3h} structure in the free ion towards a pyramidal C_{3v} configuration in the complex ($\angle$Ar–C–H≈100°).[12,23]

Complexes composed of CH_3^+ and neutral ligands X are stabilized intermediates of ion–molecule reactions with relevance to astrophysics, organic chemistry, and biology.[24–29] Hence, the characterization of the interaction in CH_3^+–X complexes provides valuable insights into the reactivity of this fundamental carbocation. In the present work the infrared spectrum of the CH_3^+–He complex has been recorded in the vicinity of the asymmetric C–H stretch vibration of the free CH_3^+ ion ($\nu_3=3108.4\,cm^{-1}$).[30] In addition, quantum chemical calculations have been conducted to characterize the intermolecular potential energy surface of this ionic com-

[a]Present address: JILA, University of Colorado, Boulder, Colorado 80309-0440.
[b]Author to whom correspondence should be addressed.

plex. The comparison between CH_3^+–He and the previously studied CH_3^+–Ar dimer provides useful information on how certain spectroscopic and dynamical properties of the interaction in CH_3^+–Rg complexes depend on the intermolecular bond strength. These include the relative stability of π-bound vs proton-bound structures, the amount of transferred charge, and the influence of the Rg ligand on the CH_3^+ monomer.

Another interesting aspect of the CH_3^+–He dimer investigated in this work concerns the angular anisotropy of its intermolecular interaction potential. This π-bound complex may be considered as a prototype of a weakly-bound ionic ''disk-and-ball'' system, similar to the neutral C_6H_6–Rg (Refs. 31 and 32) or SO_3–Rg dimers.[33] The topology of the intermolecular potential energy surface of such complexes is expected to be different from those of linear ''rod-and-ball'' [e.g., N_2H^+–He,[34,35] OCH^+–He,[36] or Ar-HCN (Ref. 37)] and ''ball-and-ball'' complexes [e.g., NH_4^+–He (Ref. 38) or Ar-HF (Refs. 39 and 40)]. For ball-and-ball systems the optimal intermolecular separation does not strongly depend on the relative orientation of the complex's constituents (though the interaction strength may do). On the other hand, in rod-and-ball and disk-and-ball dimers the optimal intermolecular bond length features usually a strong angular dependence. The main difference between these two categories is that in disk-and-ball dimers the optimal separation increases as the ligand is tilted away from the equilibrium position, whereas linear rod-and-ball complexes display the opposite behavior. The dependence of the optimal intermolecular separation on the intermolecular angular coordinates is usually referred to as angular-radial coupling.[40] This phenomenon can have an important influence on the rotational constants of weakly-bound complexes, as they are vibrationally averaged quantities.[40,41] The present work examines the spectroscopic consequences of the disk-and-ball signatures of the CH_3^+–He intermolecular potential.

A further topic investigated in the present study deals with the magnitude of the angular anisotropy of intermolecular potentials in ionic He-containing complexes. The anisotropy can vary drastically from complex to complex and its correlations with the intermolecular bond strength and monomer structure have not been explored in detail. For example, the intermolecular interaction in linear proton-bound dimers of the form AH^+–He appears to be very directional [e.g., OH^+–He (Refs. 18, 42) or N_2H^+–He (Refs. 34, 35)] with large barriers for internal rotation and relatively small zero-point angular excursions. On the other hand, the interaction potential in NH_4^+–He is more isotropic, with almost no barrier for internal rotation.[38] The planar CH_3^+ ion constitutes an intermediate case between linear and tetrahedral ionic cores, and the presented spectrum of the CH_3^+–He complex, together with the *ab initio* calculations, provides valuable information about the magnitude of the angular anisotropy of its prototype disk-and-ball interaction potential.

II. EXPERIMENT

The IR photodissociation spectrum of the CH_3^+–He complex has been recorded in a tandem mass spectrometer apparatus described in detail elsewhere.[10,43] The cluster ion source comprises a pulsed supersonic expansion which is crossed by two electron beams close to the nozzle orifice. The employed gas mixture contained CH_4, H_2, and He in a ratio of approximately 1:1:1100 at a stagnation pressure of 8 bar. Electron impact ionization of the gas mixture is followed by ion–molecule and clustering reactions to form cold ionic complexes. Part of the plasma was extracted through a skimmer into a quadrupole mass spectrometer (QMS) which was tuned to the mass of CH_3^+–He (19 u). The mass-selected CH_3^+–He beam was injected into an octopole ion guide where it was overlapped in space and time with the IR laser pulse. Excitation into metastable rovibrational levels above the lowest dissociation threshold caused the fragmentation of the CH_3^+–He complexes into CH_3^+ ions and He atoms. A second QMS served as a filter for the produced CH_3^+ fragment ions (15 u), which were subsequently detected by a Daly-type ion detector. Photofragmentation spectra were recorded by measuring the fragment ion current as a function of the laser frequency.

Tunable IR radiation was produced by an optical parametric oscillator (OPO) based laser system. The calibration of the laser frequency was accomplished by simultaneously recording etalon markers of the oscillator of the OPO and optoacoustic spectra of NH_3.[44] The absolute accuracy of the calibration is limited to approximately 0.01 cm^{-1} by the laser bandwidth (0.02 cm^{-1}) and the uncertainty of the kinetic energy of the parent ions in the octopole region. For further details of the experimental procedure, the reader is referred to the recent study of CH_3^+–Ar_n.[12]

III. *AB INITIO* CALCULATIONS

Ab initio calculations have been performed for CH_3^+ and CH_3^+–He to determine the salient attributes of the intermolecular bond, as well as the influence of the He ligand on the intramolecular properties of the CH_3^+ ion. The calculations serve not only as a basis for comparison with available experimental data, but also provide information on the interaction potential not probed experimentally (e.g., potential barriers, structure, and stability of isomeric structures). In addition to CH_3^+–He, the N_2H^+–He complex has been studied at the same level of theory to investigate the difference in the topology of the intermolecular interaction potentials acting in ionic complexes with π-bound and proton-bound equilibrium structures.

Most of the calculations were performed at the MP2 level of theory using the GAUSSIAN 94 program package.[45] The employed basis set, abbreviated as aug-cc-pVTZ# in the present work, was composed of Ahlrichs VTZ basis functions for the core electrons, augmented with diffuse and polarization functions taken from the aug-cc-pVTZ basis set.[46] The contraction scheme can be described as follows: $(11s7p3d2f) \rightarrow [7s4p3d2f]$ for C and N, and $(6s3p2d) \rightarrow [4s3p2d]$ for H and He. If not stated otherwise, all coordinates were allowed to relax during the search for stationary points. For the determination of the intermolecular well depths, D_e, the calculated interaction energies were corrected for basis set superposition error (BSSE).[47] The energies derived in this way (E_1) were further corrected for the

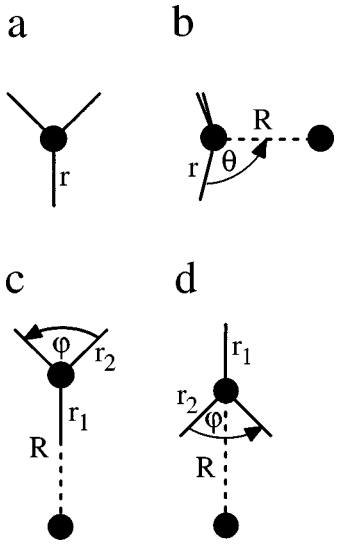

FIG. 1. Calculated structures of CH_3^+ (a, D_{3h}) and CH_3^+–He (b–d). The π-bound structure of the dimer corresponds to the global minimum (b, C_{3v}), the vertex-bound planar structure is a local minimum (c, C_{2v}) and the side-bound geometry represents a saddle point (d, C_{2v}).

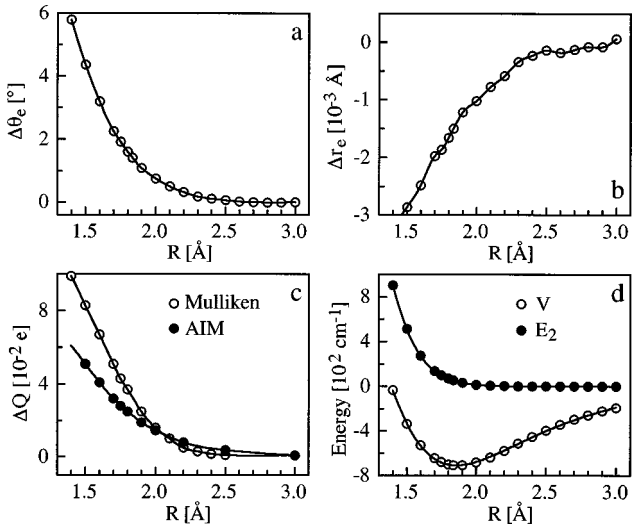

FIG. 2. Various properties of the CH_3^+–He complex (C_{3v}) as a function of the intermolecular separation R, calculated at the MP2/aug-cc-pVTZ# level of theory; (a) $\Delta\theta_e=\theta_e-90°$; (b) $\Delta r_e=r_e^{\text{complex}}-r_e^{\text{monomer}}$; (c) transferred charge ΔQ from He to CH_3^+ according to Mulliken and AIM population analysis; (d) intermolecular potential energy (V) and relaxation energy (E_2).

relaxation energy (E_2) caused by the complexation-induced deformation of the CH_3^+ unit.[48] The results of the calculations are summarized in Figs. 1–4 and Tables I and II. Harmonic vibrational frequencies were scaled by a factor 0.9437 to bring the calculated ν_3 frequency of CH_3^+ in agreement with the experimental value ($\nu_3=3108.4\,\text{cm}^{-1}$).[30] As the CH_3^+ vibrational modes are only slightly modified upon He complexation, the employed nomenclature for the complex's normal modes refers to the four intramolecular modes of CH_3^+ ($\nu_1-\nu_4$) and the intermolecular stretching and bending vibrations (ν_s and ν_b).

The calculated equilibrium geometry of CH_3^+ corresponds to a planar structure with D_{3h} symmetry [Fig. 1(a)]. Both the C–H bond length (r_e) and the scaled vibrational frequencies ($\nu_1-\nu_4$), show satisfying agreement with available experimental data[30,49,50] (Table I) and the results of previous calculations,[51,52] suggesting that the chosen level of theory is sufficient for the description of the monomer properties.

Similar to the CH_3^+–Ar dimer, the π-bound configuration of CH_3^+–He corresponds to the global minimum structure of the complex [Fig. 1(b), Table II]. The intermolecular bond is characterized by $R_e=1.834$ Å and $D_e=707\,\text{cm}^{-1}$. The CH_3^+ unit experiences modest geometry changes upon complexation, as is evidenced by the deformation energy of $E_2=55\,\text{cm}^{-1}$. The ion becomes slightly nonplanar ($\theta_e=91.4°$) and the C–H bonds contract somewhat ($\Delta r_e=-0.0015$ Å) leading to a small increase in the C–H stretching frequencies ($\Delta\nu_1=12.5\,\text{cm}^{-1}$, $\Delta\nu_3=13.2\,\text{cm}^{-1}$). According to the Mulliken population analysis, which gave similar results as the less basis set dependent atoms-in-molecules (AIM) analysis,[53,54] there is only little charge transfer from He to CH_3^+ involved in the bond formation ($\Delta Q\approx 0.03-0.04\,e$), implying that induction forces dominate the attractive part of the intermolecular potential. This is in contrast to CH_3^+–Ar where substantial charge transfer ($\Delta Q\approx 0.3\,e$) contributes to the stabilization of the π-bonded configuration.[12]

To investigate the influence of He complexation on the CH_3^+ monomer, several properties of the complex have been calculated for different intermolecular separations R, with the He atom approaching the CH_3^+ ion along the C_3 axis. Figure 2 shows the R dependencies of the CH_3^+ structure (r_e, θ_e), the transferred charge (ΔQ), and the interaction and relaxation energies (V and E_2). Comparison of these plots with the corresponding data for CH_3^+–Ar reveals that, though the dependencies are qualitatively similar for both complexes,

TABLE I. Calculated CH bond length (r_e) and scaled harmonic frequencies of CH_3^+ (D_{3h}) compared to available experimental values. IR intensities (in km/mol) and vibrational symmetry species are given in parentheses.

Level	r_e (Å)	B_e (cm^{-1})	C_e (cm^{-1})	ν_1 (cm^{-1})	ν_2 (cm^{-1})	ν_3 (cm^{-1})	ν_4 (cm^{-1})
MP2/aug-cc-VTZ#	1.0844	9.482 899	4.741 450	2917.9	1360.2	3108.4	1365.3
				(a_1'/0.0)	(a_2''/7)	(e'/148)	(e'/34)
expt	~1.087[a]				1380±20[b]	3108.4[a]	

[a]Reference 30.
[b]Reference 49.

TABLE II. Structure, rotational constants, energetics, and scaled harmonic frequencies of several CH_3^+–He isomers [Figs. 1(b)–(d)] calculated at the MP2/aug-cc-pVTZ# level. IR intensities (in km/mol) and vibrational symmetry species are given in parentheses.

Structure	r_e (r_{1e}/r_{2e}) (Å)	R_e (Å)	θ_e/φ_e	A_e (cm^{-1})	B_e (cm^{-1})	C_e (cm^{-1})	E_1 (cm^{-1})	E_2 (cm^{-1})	D_e (cm^{-1})
π-bound (C_{3v})	1.0829	1.8337	91.4°	4.757 86	1.352 609	1.352 609	761.6	54.5	707.1
vertex-bound (C_{2v})	1.0846/1.0844	3.3650	119.9°	9.487 73	0.448 727	0.428 462	112.8	<0.1	112.8
side-bound (C_{2v})	1.0844/1.0843	3.1269	119.9°	9.494 56	0.515 856	0.489 273	108.6	<0.1	108.6

Structure	ν_1 (cm^{-1})	ν_2 (cm^{-1})	ν_3 (cm^{-1})	ν_4 (cm^{-1})	ν_s (cm^{-1})	ν_b (cm^{-1})
π-bound	2930.4	1337.4	3121.6	1361.2	193.2	569.6
(C_{3v})	(a_1/0.4)	(a_1/2)	(e/140)	(e/33)	(a_1/51)	(e/3)
vertex-bound	2916.4	1361.2	3105.4	1367.3	84.6	68.5
(C_{2v})	(a_1/0.4)	(b_1/7)	(a_1/87)	(a_1/16)	(a_1/17)	(b_1/0.5)
			3108.4	1366.1		27.6
			(b_2/73)	(b_2/16)		(b_2/1)
side-bound	2918.4	1360.1	3109.1	1363.2	73.7	i47.9
(C_{2v})	(a_1/0.0)	(b_1/7)	(a_1/74)	(a_1/19)	(a_1/16)	(b_1/0.7)
			3109.4	1364.3		18.8
			(b_2/72)	(b_2/18)		(b_2/2)

they are much more pronounced for CH_3^+–Ar due to the significantly stronger intermolecular interaction.[12]

Two further stationary points on the CH_3^+–He intermolecular potential energy surface have been investigated; the vertex-bound local minimum [Fig. 1(c)] and the side-bound transition state [Fig. 1(d)]. Both planar geometries have C_{2v} symmetry and feature much weaker and longer intermolecular bonds compared to the global minimum (Table II). The changes in the CH_3^+ properties induced by the He complexation are therefore very small for these planar structures. The difference in the binding energies of the π-bound and planar geometries indicate that the barrier for internal rotation of the CH_3^+ unit within the complex is of the order of 600 cm^{-1}. The resulting large angular anisotropy of the intermolecular potential keeps the He atom localized in the π-bound region near the $2p_z$ orbital of the C atom. The high intermolecular bending frequency of the π-bonded equilibrium structure, $\nu_b = 570\ cm^{-1}$, is a further signature for the steep rise in the intermolecular potential along the angular coordinates. One-dimensional hindered rotor simulations indicated that a barrier of 600 cm^{-1} for the internal rotation of the CH_3^+ unit around its a (or b) axis causes only small tunneling splittings (<0.0005 cm^{-1}). On the other hand, both planar H-bonded structures have very similar binding energies and low-frequency in-plane bending modes ($\nu_b = 28$ and 19 cm^{-1}, Table II), indicating that the He atom experiences almost no barrier when moving in the molecular plane along the minimum energy path around the CH_3^+ ion. In general, the topology of the CH_3^+–He intermolecular potential energy surface is similar to that of CH_3^+–Ar, with the major difference being that the interaction in the latter complex is roughly one order of magnitude stronger.[12]

Selected parts of the three-dimensional intermolecular potential energy surface of CH_3^+–He were studied in more detail. In these calculations the structure of the CH_3^+ monomer was kept rigid (rigid monomer approximation, $r_e = 1.0844$ Å). Interaction energies were calculated for a grid of intermolecular coordinates R and γ, where γ measures the deviation of the He–C–H angle from 90° and R the intermolecular He–C separation (Fig. 3). For each angle (γ=0°, ±5°, ±10°, ±20°, ±45°, ±67.5°, ±90°), the energies of at least 10 radial points (spaced by 0.1 Å) were least-squares fitted to an analytical function, consisting of (i) an exponential term $\exp(-\alpha R)$ describing the exchange repulsion and (ii) a β/R^4 term representing the attractive charge-induced dipole interaction.[55] Minimum energies (D_{min}) and the corresponding separations (R_{min}) of these one-dimensional ra-

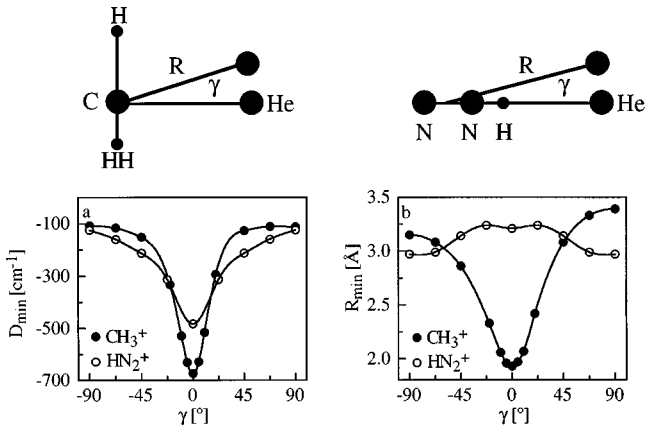

FIG. 3. Selected properties of the intermolecular potential energy surface of the CH_3^+–He and N_2H^+–He complexes calculated at the MP2/aug-cc-pVTZ# level of theory (rigid monomer approximation). Plotted are the potential energy depths (D_{min}) and minimal energy separations (R_{min}) of the one-dimensional radial cuts through the intermolecular potential energy surfaces as a function of the bending angle γ.

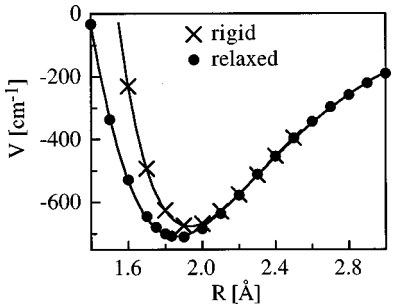

FIG. 4. One-dimensional radial cuts through the CH_3^+–He intermolecular potential energy surface along the C_{3v} symmetry axis for fixed and relaxed CH_3^+ internal coordinates. Monomer relaxation leads to a slightly stronger and shorter intermolecular bond.

dial cuts through the three-dimensional intermolecular potential energy surface are plotted in Fig. 3 as a function of γ. In the vicinity of the π-bound global minimum ($\gamma=0°$) the potential is quite steep along the bending coordinate [Fig. 3(a)] and features strong coupling between radial and angular intermolecular coordinates [Fig. 3(b)]. Already small angular elongations lead to a significant increase in $R_{\min}$ and a decrease in the interaction strength $D_{\min}$. The massive angular anisotropy is in accordance with the large calculated intermolecular bending frequency ($\nu_b=570\,\mathrm{cm}^{-1}$), which exceeds by far the one of the intermolecular stretching mode ($\nu_s=193\,\mathrm{cm}^{-1}$). Moreover, the plots are only slightly asymmetric with respect to γ, indicating that the intermolecular potential is relatively independent of the azimuthal angle ($\gamma=90°$ and $-90°$ correspond to the vertex-bound and side-bound structures, see Fig. 1).

The N_2H^+–He intermolecular potential energy surface has been explored with the same methods and the results are compared in Fig. 3 with the corresponding CH_3^+–He data.[55] The monomer geometry was fixed at $r_{NN}=1.1058\,$Å and $r_{NH}=1.0331\,$Å and radial points were calculated for $\gamma=0°$, 22.5°, 45°, 67.5°, and 90° (the N_2H^+–He potential is symmetric in γ). Similar to the CH_3^+–He complex, the surface of N_2H^+–He features a pronounced minimum at $\gamma=0°$, in agreement with previous spectroscopic data[34] and *ab initio* calculations.[35] However, the minimum is less steep for elongations along the bending coordinate [Fig. 3(a)] and the $R_{\min}$ dependence on γ is much smaller than in the case of CH_3^+–He [Fig. 3(b)].

To visualize the effect of the rigid monomer approximation on the shape of the intermolecular potential, the radial potential obtained for $\gamma=0°$ by relaxing the monomer coordinates r and θ is compared with the corresponding rigid monomer cut in Fig. 4. As expected, the main differences are observed in the short range part of the potential function, where the relaxation of the CH_3^+ internal coordinates leads to a substantial additional stabilization. However, the effects on D_e and R_e are less pronounced ($D_e=709$ vs 676 cm^{-1} and $R_e=1.86$ vs 1.93 Å for relaxed vs rigid monomer potential). The minimum of the relaxed surface features a slightly longer bond than that obtained by the gradient optimization method ($D_e=707\,\mathrm{cm}^{-1}$, $R_e=1.83\,$Å, Table II), as the former corresponds to the minimum on the BSSE corrected surface while the latter one is that on the uncorrected surface.[48,56] The effects of monomer relaxation on $D_{\min}$ and $R_{\min}$ decrease as $|\gamma|$ increases, because the intermolecular interaction becomes weaker. As relaxation of the internal monomer coordinates during complex formation gives rise to an additional contribution to the binding energy of up to $\approx$50 cm^{-1} (7%), future efforts to explore the properties of the intermolecular interaction in CH_3^+–He in a more quantitative way will require a potential energy surface that takes monomer relaxation into account.

To test whether the MP2/aug-cc-pVTZ# level of theory is sufficient for a reliable description of the interaction in the CH_3^+–He complex, minima on the rigid monomer surface have also been calculated at the MP4/aug-cc-pVTZ# ($r_e=1.0877\,$Å, $R_e=1.8897\,$Å, $D_e=727\,\mathrm{cm}^{-1}$) and MP2/aug-cc-pVQZ ($r_e=1.0827\,$Å, $R_e=1.8939\,$Å, $D_e=712\,\mathrm{cm}^{-1}$) levels of theory. Comparison with the corresponding results obtained at the MP2/aug-cc-pVTZ# level ($r_e=1.0844\,$Å, $R_e=1.9049\,$Å, $D_e=675\,\mathrm{cm}^{-1}$) indicates that increasing either the basis set size or the level of theory for the treatment of electron correlation leads only to a modest increase in the calculated interaction energy. These observations suggest that the MP2/aug-cc-pVTZ# level is adequate for a near quantitative determination of the intermolecular potential energy surface of the CH_3^+–He complex.

IV. EXPERIMENTAL RESULTS

The mid-infrared photodissociation spectrum of the CH_3^+–He complex has been recorded between 3080 and 3170 cm^{-1} to search for the strong IR active ν_3 fundamental and within the scanned range only one intense transition has been found (Fig. 5). Both the vibrational frequency ($\approx$3115 cm^{-1}) and the rotational structure of the observed transition are consistent with an assignment to the ν_3 fundamental of a π-bound CH_3^+–He complex.

The rotational structure of the observed band is characteristic of a perpendicular transition of a prolate symmetric top, with Q branches of adjacent $\Delta K=\pm1$ subbands spaced by approximately $2[A(1-\xi_3)-B)]\approx6.5\,\mathrm{cm}^{-1}$. Neighboring subbands are heavily overlapping, as the B rotational constant (≈1 cm^{-1}) is only about 4–5 times smaller than A and rotational cooling is not complete ($T_{\mathrm{rot}}\approx30\,$K). The assignment of the J and K rotational quantum numbers to the energy levels involved in the observed transitions were based on the relative intensities of the unresolved Q branches ($^rQ_0$ being the most intense) and missing P and R branch lines involving levels with $J<K$. In total, 68 rotational line positions, ranging from $K=0$ to 5 and $J=0$ to 9,[55] were least-squares fitted to a standard semirigid symmetric top Hamiltonian, including the first order Coriolis coupling term for the twofold degenerate upper vibrational level ($l=0$ for $v_3=0$, $l=\pm1$ for $v_3=1$),[57]

$$E(J,K)=\nu_0+BJ(J+1)+(A-B)K^2-D_JJ^2(J+1)^2$$
$$-D_{JK}J(J+1)K^2-D_KK^4-2\xi lAK.$$

Table III summarizes the obtained molecular constants for the ground and ν_3 vibrational states. The standard deviation

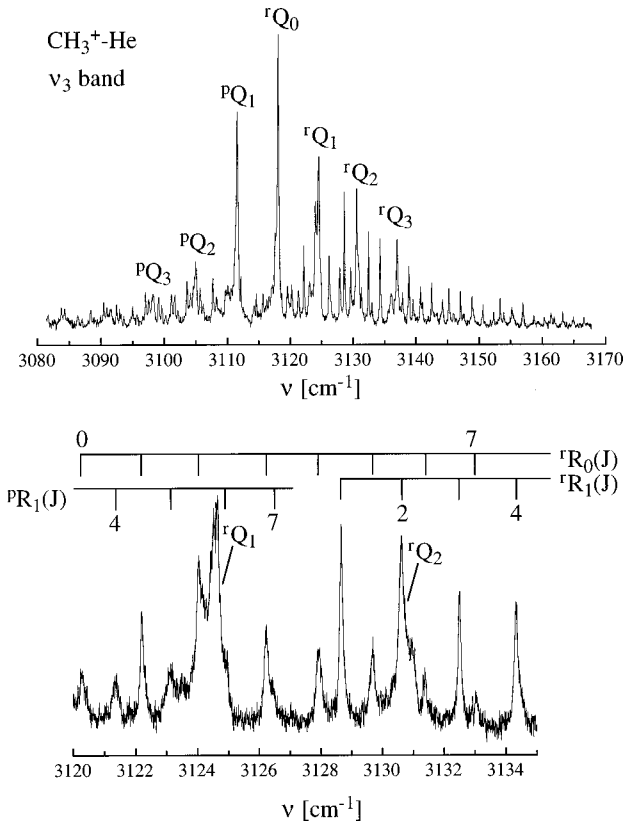

FIG. 5. Photodissociation spectrum of the ν_3 fundamental of the CH_3^+–He complex. The structure of the band is characteristic of a perpendicular transition of a prolate symmetric top. In the top panel the assignments of the unresolved Q branches of the individual $\Delta K=\pm 1$ subbands are indicated. The bottom panel shows an expanded portion of the spectrum with the assignments for individual rovibrational transitions. The employed notation corresponds to ${}^{\Delta K}\Delta J_K(J)$. The line width of the narrowest individual line is $\approx$0.12 cm^{-1} (FWHM).

of the fit (0.03 cm^{-1}) is of the order of the laser resolution (0.02 cm^{-1}) and well below the line width of the observed transitions (0.12 cm^{-1}).

V. DISCUSSION

A. Structural and dynamical properties of CH_3^+–He

The structure of the observed spectrum and the derived rotational constants show that the CH_3^+–He dimer has a π-bonded equilibrium geometry [C_{3v} symmetry, Fig. 1(b)], in agreement with the *ab initio* calculations. In this structure all three protons are equivalent, giving rise to a double nuclear spin statistical weight for levels with $K=3n$ ($n>0$). This intensity alternation can be discerned in the observed spectrum, though it is not very distinct, probably due to the nonthermal population of rotational levels usually observed in the employed cluster ion source.[18,58] On the other hand, for a rigid planar C_{2v} structure a more pronounced 3:1 intensity alternation for adjacent Q branches is anticipated, but not observed in the spectrum. For a rigid C_{2v} complex the ν_3 fundamental should also be split into a parallel and perpendicular component with roughly equal intensity (Table II), in disagreement with the experimental observation. In addition, the derived rotational constants are not compatible with a rigid planar structure or a complex featuring free internal rotation of CH_3^+.

Single rotational transitions in the ν_3 spectrum have a linewidth of $\approx$0.12 cm^{-1}, which is significantly larger than the bandwidth of the employed laser (0.02 cm^{-1}). The observed broadening may be caused by either power broadening or a short lifetime of the excited ν_3 state of the complex. The former mechanism is not very likely as reducing the laser intensity by a factor of 5 did not affect the observed linewidths (further intensity attenuation resulted in an impractically low signal to noise ratio). Assuming that the line broadening arises from rapid intracluster vibrational energy redistribution and/or predissociation, the lifetime of the ν_3 vibrational state can be estimated as $\approx$50 ps. A similar short lifetime of 38 ps has been determined for the ν_1 level of N_2H^+–He,[34] whereas the ν_1 lifetimes of the related proton-bound complexes OH^+–He (Ref. 18) and OCH^+–He (Ref. 36) exceed 200 ps.

The molecular constants in Table III can be used to determine several properties of the intermolecular bond in the ground and ν_3 vibrational states of the CH_3^+–He complex.[59] Treating the dimer as a pseudodiatomic molecule yields an averaged intermolecular separation $R_{cm}=R_{C-He}=2.176(3)$ Å for the ground state, under the assumption that the CH_3^+ unit is not distorted upon complexation ($B_{CH_3^+}\approx 9.3622\,cm^{-1}$ for $v_3=0$, $B_{CH_3^+}\approx 9.2724\,cm^{-1}$ for $\nu_3=1$).[50] The slight monomer distortion predicted by the *ab initio* calculations, namely a CH bond contraction of 0.0015 Å and a 1.4° deviation from planarity, has only a minor effect on the inferred C–He separation ($R_{cm}-R_{C-He}<0.008$ Å). The harmonic force constant and frequency of the intermolecular stretching mode amount to $k_s=2.4(2)$ N/m and $\omega_s=113(4)$ cm^{-1}. Excitation of ν_3 causes a very slight decrease in the intermolecular interaction strength, as evidenced by the longer and weaker intermolecular bond in the $\nu_3=1$ state [$R_{cm}=2.187(2)$ Å, $k_s=2.2(2)$ N/m, $\omega_s=109(4)$ cm^{-1}] and the $\approx$7 cm^{-1} blue shift of the ν_3 frequency upon complexation.

Comparison of the calculated equilibrium structure and harmonic vibrational frequencies with the experimentally inferred values may suggest that the MP2/aug-cc-pVTZ# calculations significantly overestimate the intermolecular bond strength. Indeed, they predict a much shorter C–He bond ($R_e=1.83$ Å vs $R_{cm}=2.18$ Å), a higher intermolecular

TABLE III. Determined molecular constants (in cm^{-1}) of the ground and ν_3 vibrational states of the CH_3^+–He complex. Numbers in parentheses represent 2σ limits.

$\nu_3-\xi_3 A'$	3115.047(18)[a]
B''	1.0053(19)
$D_j''\times 10^4$	2.82(18)
$D_{jk}''\times 10^4$	−4.5(1.6)
$D_k''\times 10^4$	5.4(3.2)
$A'(1-\xi_3)$	4.2356(52)
$A'-A''$	−0.0391(34)
B'	0.9954(19)
$D_j'\times 10^4$	2.97(19)
$D_{jk}'\times 10^4$	−4.4(1.1)
$D_k'\times 10^4$	4.2(1.7)

[a]Absolute uncertainty is ± 0.01 cm^{-1}.

stretching frequency (193 vs 113 cm^{-1}), and a larger complexation-induced blue shift for ν_3 (13.2 vs 7 cm^{-1}). However, increasing the level of theory or the basis set size was shown to only slightly increase the intermolecular interaction compared to the results obtained at the MP2/aug-cc-pVTZ# level ($\Delta R_e < 0.02$ Å, see Sec. III). These results suggest that the massive discrepancy between calculated and observed values for the intermolecular separation ($R_{cm} - R_e = 0.35$ Å) may arise from other sources, such as large amplitude zero-point motions in the ground vibrational state of the complex, rather than an insufficient level of theory employed for the calculation of the potential energy surface.

To estimate the effects of the zero-point motions along the intermolecular bending and stretching coordinates on the vibrationally averaged ground state geometry of the complex, the calculated cuts through the three-dimensional intermolecular potential are considered. For the radial motion, eigenvalues and eigenfunctions of the one-dimensional radial potential (relaxed monomer, Fig. 4) have been determined by solving the Schrödinger equation using the LEVEL program and treating the CH_3^+–He complex as a diatomic molecule.[60] The anharmonicity of this potential reduces the harmonic frequency $\omega_s = 205\ cm^{-1}$ (unscaled value) to $\nu_s = 175\ cm^{-1}$ (fundamental) and leads to an averaged ground state intermolecular separation that is ≈0.05 Å longer than the equilibrium separation. Thus, the radial motion provides only a minor contribution to the observed difference of $R_{cm} - R_e \approx 0.35$ Å.

The calculated intermolecular bending frequency of $\omega_b = 604\ cm^{-1}$ (unscaled value) corresponds in the two-dimensional isotropic harmonic oscillator approximation to an average elongation of $\langle \gamma^2 \rangle^{1/2} = 11°$. According to the rigid monomer surface, the minimum along the nearby $\gamma = 10°$ radial cut lies at $R_{min} = 2.07$ Å ($R_{min} = 2.06$ Å for $\gamma = -10°$). The effective rotational constant of this structure, $B_{eff} = 1/2(B + C) = 1.07\ cm^{-1}$, is much closer to the experimental value, $B_0 = 1.0053\ cm^{-1}$, than the equilibrium value, $B_e = 1.35\ cm^{-1}$ (Table II). These results imply that it is mainly the intermolecular bending vibration that causes the effective averaged intermolecular separation (R_{cm}) in the vibrational ground state of the CH_3^+–He complex to be much larger than the calculated equilibrium distance (R_e). A more quantitative analysis of the effects of zero-point motions on the spectroscopic constants of the complex requires the solution of the Schrödinger equation using a three-dimensional intermolecular potential energy surface.

B. Comparison with related ionic complexes

The intermolecular potential energy surface of the CH_3^+–He complex may be compared with previously studied cluster ions of the type AH^+–He. In cases of linear AH^+ ions, where A has a relatively low PA ($PA_A = 485$, 494, and 594 kJ/mol for A = O, N_2, and CO),[61] the potential energy surfaces of the corresponding AH^+–He complexes feature pronounced global minima at linear proton-bound configurations. Their intermolecular force constants and binding energies are anticorrelated with the PA of A; $k_s = 6.16$, 4.81, and 1.64 N/m and $D_e = 650$, ≈530, and ≈250 cm^{-1} for OH^+–He,[18] N_2H^+–He,[34] and HCO^+–He,[36,62] respectively. In contrast to these linear rod-and-ball complexes, which feature large barriers for internal rotation, the angular anisotropy in NH_4^+–He is very small.[38] The high PA of NH_3 (854 kJ/mol) (Ref. 61) allows only for a weak bond ($D_e \approx 150\ cm^{-1}$) and, though the He atom appears to slightly favor proton-bound sites, the interaction of the He atom with the tetrahedral NH_4^+ ion is rather isotropic. The similarly high PA of CH_2 (837 kJ/mol) (Ref. 63) is also responsible for the weak and nearly isotropic interaction in planar CH_3^+–He configurations ($D_e \approx 110\ cm^{-1}$). However, the intermolecular interaction in CH_3^+–He complex strongly favors the π-bound structure ($D_e \approx 700\ cm^{-1}$) over the planar H-bonded configurations [Fig. 3(a)], and the large angular anisotropy of the intermolecular potential locks the He atom in that region.

The angular-radial coupling effects observed in CH_3^+–He are much larger than in linear proton-bound complexes with He (e.g., OH^+–He or N_2H^+–He).[18,34,35,42] In those linear rod-and-ball systems the zero-point bending motion has only a minor effect on the effective intermolecular separation [see Fig. 3(b) for N_2H^+–He], as the dependence of R_{min} on the angle γ is weak near the equilibrium value ($\gamma < 30°$). This is in contrast to CH_3^+–He, where already small bending elongations increase the separation of the He atom from the C atom and even from the CH_3^+ plane. Zero-point effects in the radial coordinate are similar in both types of complexes, as the interaction strengths are comparable [Fig. 3(a)]. They lead to a moderate elongation of the effective intermolecular separation by some 0.05 Å. As a result, the R_e and R_{cm} values differ by less than 0.05 Å for linear proton-bound complexes, mainly owing to zero-point elongations along the stretching coordinate, while in the case of the CH_3^+–He complex the difference is much larger (0.35 Å) due to the substantial additional contribution arising from the bending coordinate.

The properties of the CH_3^+–He complex may be compared with those of the related CH_3^+–Ar dimer.[12] Both complexes have a π-bound equilibrium structure. However, the Ar complex has a much stronger intermolecular bond ($D_e = 6411$ vs 707 cm^{-1}, MP2/aug-cc-pVTZ#). The eightfold larger polarizability of Ar compared to He causes stronger induction interactions with the charge distribution in CH_3^+ and, as Ar is a better electron donor than He, the π-bound configuration can gain significant additional stabilization via a partial charge transfer from the rare gas atom into the vacant electrophilic $2p_z$ orbital of C ($\Delta Q = 0.3$ vs $0.03\,e$). The stronger bond to the Ar ligand causes a much larger perturbation on the structure of CH_3^+ ($\Delta r_e = -0.005$ vs -0.0015 Å, $\Delta\theta_e = 9.6°$ vs 1.4°), which is also visible in a larger deformation energy ($E_2 = 2501.2$ vs 54.5 cm^{-1}). In the language of valence bond theory, the sp^2 hybridization of C in CH_3^+ is much more transformed towards sp^3 hybridization in the case of Ar due to the enhanced charge transfer. In general, the CH_3^+–Ar complex is closer to the isoelectronic CH_3Cl molecule (concerning structure, bond energies and vibrational frequencies), than CH_3^+–He is to isoelectronic CH_4.

The experimental ν_3 frequency of the CH_3^+–He complex ($\approx$3115 cm^{-1}) is bracketed by those of the bare CH_3^+ and CH_3 molecules (3108.4 and 3160.8 cm^{-1}).[30,64] It is, however, much closer to the former value, supporting the conclusion of a small charge transfer from He to the CH_3^+ ion. The ν_3 frequency of the CH_3^+–Ar complex could not be measured directly by predissociation spectroscopy, as the ν_3 level lies below the dissociation energy.[12] Observed sequence bands of the type $\nu_x+\nu_3 \leftarrow \nu_x$ gave, however, an approximate value of $\nu_3 \approx 3145\,cm^{-1}$, which is close to the *ab initio* frequency (3136 cm^{-1}) and the value obtained from a fit of measured CH stretch overtone and combination band frequencies to a local mode model (3132 cm^{-1}).[12] The higher ν_3 frequency of CH_3^+–Ar compared to CH_3^+–He is in accordance with the larger charge transfer involved in the formation of the intermolecular bond.

For many stable species a nearly linear correlation between their proton and methyl cation affinities (PA-MCA) has been established, and the noble gases Kr (PA=427 kJ/mol, MCA=200 kJ/mol) and Xe (PA=500 kJ/mol, MCA =231 kJ/mol) were found to follow this relationship.[65] Further extrapolation of this rule to the rare gas atoms Ar, Ne, and He predict their MCAs as 175, 103, and 94 kJ/mol from their respective PAs (369, 199, and 178 kJ/mol).[61] The MCA of Ar has been measured as 47±8 kJ/mol in thermochemical experiments,[22] and this value is consistent with recent spectroscopic and *ab initio* data.[12] It is not trivial to determine the MCA of He from the present *ab initio* calculations, as the anharmonic zero-point energy contributions are difficult to estimate for this weakly-bound complex. A conservative upper limit for the MCA of He can however be derived as ≈12 kJ/mol from the relation $MCA = D_0 < D_e < 10^3\,cm^{-1}$. Apparently, the linear PA-MCA relation is not valid for Rg atoms that are smaller than Kr, as it drastically overestimates their MCAs. A possible reason for this discrepancy may result from a change in the bonding mechanism in Rg–H^+ and Rg–CH_3^+ dimers as the size of the rare gas atom increases. While all Rg–H^+ diatomics feature strong covalent bonds, only the Rg–CH_3^+ dimers with large rare gas ligands have bonds with substantial covalent character. In the case of CH_3^+–He, induction interactions dominate the attractive part of the intermolecular potential. In the case of CH_3^+–Ar, partial charge transfer provides additional stabilization of the intermolecular bond and this contribution becomes probably more important for CH_3^+–Rg complexes with larger Rg atoms.[65]

VI. CONCLUSIONS

The intermolecular interaction in the CH_3^+–He ionic complex has been investigated by quantum chemical calculations and infrared predissociation spectroscopy. The observed ν_3 spectrum of the complex is compatible with a π-bound equilibrium structure, where the He atom is attached to the $2p_z$ orbital of C. The intermolecular bond in the vibrational ground state is characterized by an averaged C–He separation of $R_{cm}=2.18$ Å and a harmonic stretching force constant of $k_s=2.4$ N/m. Excitation of ν_3 leads to a small destabilization of the intermolecular bond (≈7 cm^{-1}).

The calculated intermolecular potential energy surface of the complex features a pronounced global minimum at the π-bound configuration with a well depth of $D_e \approx 700\,cm^{-1}$ and an equilibrium separation $R_e \approx 1.85$ Å. Large angular anisotropy in the potential confines the He atom to the π-bound region. Anomalous effects of the zero-point motions on the effective intermolecular separation are caused by the special topology of the intermolecular potential. Though zero-point intermolecular bending excursions are not particularly large, they lead via large angular-radial coupling effects to an effective averaged intermolecular separation in the vibrational ground state that is much larger than the corresponding calculated equilibrium value ($R_{cm}-R_e \approx 0.35$ Å). The angular-radial couplings caused by the special shape of the potential of CH_3^+–He, a prototype ionic disk-and-ball system, are qualitatively different from those of previously studied proton-bound complexes (e.g., N_2H^+–He), which are best represented as rod-and-ball systems.

The topology of the intermolecular potential energy surface of CH_3^+–He is similar to the one of CH_3^+–Ar, for which the interaction is roughly one order of magnitude stronger.[12] However, while the attractive part of the interaction in CH_3^+–He is dominated by induction interactions, the formation of the intermolecular π-bond in CH_3^+–Ar is accompanied by substantial charge transfer from Ar into the empty electrophilic $2p_z$ orbital.[12] Future calculations and experiments on other CH_3^+–X_n complexes (e.g., X=Ne) will further improve our understanding of the bonding mechanism in systems composed of carbocations and neutral ligands.

ACKNOWLEDGMENT

This study is part of Project No. 20-49104.96 of the Swiss National Science Foundation.

[1] A. W. Castleman and R. G. Keesee, Chem. Rev. **86**, 589 (1986).
[2] B. Brutschy, Chem. Rev. **92**, 1567 (1992).
[3] Y. Marcus, *Ion Solvation* (Wiley, New York, 1985).
[4] P. Hobza and R. Zahradnik, *Intermolecular Complexes: The Role of van der Waals Systems in Physical Chemistry and in the Biodisciplines* (Elsevier, Amsterdam, 1988).
[5] E. J. Bieske and J. P. Maier, Chem. Rev. **93**, 2603 (1993).
[6] K. Müller-Dethlefs, O. Dopfer, and T. G. Wright, Chem. Rev. **94**, 1845 (1994).
[7] M. W. Crofton, J. M. Price, and Y. T. Lee, in *Clusters of Atoms and Molecules II*, edited by H. Haberland (Springer, Berlin, 1994), Vol. 56, p. 44.
[8] J. M. Lisy, in *Cluster Ions*, edited by C.-Y. Ng, T. Baer, and I. Powis (Wiley, New York, 1993), p. 217.
[9] M. A. Duncan, Annu. Rev. Phys. Chem. **48**, 69 (1997).
[10] S. A. Nizkorodov, O. Dopfer, T. Ruchti, M. Meuwly, J. P. Maier, and E. J. Bieske, J. Phys. Chem. **99**, 17118 (1995).
[11] O. Dopfer, S. A. Nizkorodov, M. Meuwly, E. J. Bieske, and J. P. Maier, Int. J. Mass Spectrom. Ion Processes **167-168**, 637 (1997).
[12] R. V. Olkhov, S. A. Nizkorodov, and O. Dopfer, J. Chem. Phys. **108**, 10046 (1998).
[13] R. V. Olkhov, S. A. Nizkorodov, and O. Dopfer, Chem. Phys. **239**, 393 (1998).
[14] M. Bogey, H. Bolvin, C. Demuynck, and J. L. Destombes, Phys. Rev. Lett. **58**, 988 (1987).
[15] Y. Ohshima, Y. Sumiyoshi, and Y. Endo, J. Chem. Phys. **106**, 2977 (1997).
[16] A. Carrington, D. I. Gammie, A. M. Shaw, S. M. Taylor, and J. M. Hutson, Chem. Phys. Lett. **260**, 395 (1996).
[17] S. A. Nizkorodov, Y. Spinelli, E. J. Bieske, J. P. Maier, and O. Dopfer, Chem. Phys. Lett. **265**, 303 (1997).

[18] D. Roth, S. A. Nizkorodov, J. P. Maier, and O. Dopfer, J. Chem. Phys. **109**, 3841 (1998).
[19] M. Meot-Ner, J. Am. Chem. Soc. **106**, 1257 (1984).
[20] C. Lifshitz, in *Cluster Ions*, edited by C. Y. Ng, T. Baer, and I. Powis (Wiley, New York, 1993), p. 121.
[21] O. Dopfer, R. V. Olkhov, D. Roth, and J. P. Maier, Chem. Phys. Lett. **296**, 585 (1998).
[22] K. Hiraoka, I. Kudaka, and S. Yamabe, Chem. Phys. Lett. **178**, 103 (1991).
[23] A. Cunje, C. F. Rodriquez, D. K. Bohme, and A. C. Hopkinson, J. Phys. Chem. A **102**, 478 (1998).
[24] *Carbonium Ions I*, edited by G. A. Olah and P. R. Schleyer (Wiley, New York, 1968).
[25] *Carbonium Ions II*, edited by G. A. Olah and P. R. Schleyer (Wiley, New York, 1970).
[26] D. Smith and N. G. Adams, Chem. Phys. Lett. **54**, 535 (1978).
[27] T. B. McMahon, T. Heinis, G. Nicol, J. K. Hovey, and P. Kebarle, J. Am. Chem. Soc. **110**, 7591 (1988).
[28] D. M. Sonnenfroh and J. M. Farrar, J. Chem. Phys. **85**, 7167 (1986).
[29] G. P. Ford and J. D. Scribner, J. Am. Chem. Soc. **105**, 349 (1983).
[30] M. W. Crofton, M.-F. Jagod, B. D. Rehfuss, W. A. Kreiner, and T. Oka, J. Chem. Phys. **88**, 666 (1988).
[31] T. Brupbacher, J. Makarewicz, and A. Bauder, J. Chem. Phys. **101**, 9736 (1994).
[32] A. van der Avoird, P. E. S. Wormer, and R. Moszynski, Chem. Rev. **94**, 1931 (1994).
[33] D. L. Fiacco, B. Kirchner, W. A. Burns, and K. R. Leopold, J. Mol. Spectrosc. **191**, 389 (1998).
[34] M. Meuwly, S. A. Nizkorodov, J. P. Maier, and E. J. Bieske, J. Chem. Phys. **104**, 3876 (1996).
[35] M. Meuwly and R. J. Bemish, J. Chem. Phys. **106**, 8672 (1997).
[36] S. A. Nizkorodov, J. P. Maier, and E. J. Bieske, J. Chem. Phys. **103**, 1297 (1995).
[37] S. Drucker, A. L. Cooksy, and W. Klemperer, J. Chem. Phys. **98**, 5158 (1993).
[38] O. Dopfer, S. A. Nizkorodov, M. Meuwly, E. J. Bieske, and J. P. Maier, Chem. Phys. Lett. **260**, 545 (1996).
[39] J. M. Hutson, J. Chem. Phys. **96**, 6752 (1992).
[40] K. R. Leopold, G. T. Fraser, S. E. Novick, and W. Klemperer, Chem. Rev. **94**, 1807 (1994).
[41] D. J. Nesbitt and R. Naaman, J. Chem. Phys. **91**, 3801 (1989).
[42] M. Meuwly, J. P. Maier, and P. Rosmus, J. Chem. Phys. **109**, 3850 (1998).
[43] E. J. Bieske, J. Chem. Soc., Faraday Trans. **91**, 1 (1995).
[44] G. Guelachvili and K. N. Rao, *Handbook of Infrared Standards* (Academic, London, 1993).
[45] M. J. Frisch, G. W. Trucks, H. B. Schlegel, P. M. W. Gill, B. G. Johnson, M. A. Robb, J. R. Cheeseman, T. Keith, G. A. Petersson, J. A. Montgomery, K. Raghavachari, M. A. Al-Laham, V. G. Zakrzewski, J. V. Ortiz, J. B. Foresman, J. Cioslowski, B. B. Stefanov, A. Nanayakkara, M. Challacombe, C. Y. Peng, P. Y. Ayala, W. Chen, M. W. Wong, J. L. Andres, E. S. Replogle, R. Gomperts, R. L. Martin, D. J. Fox, J. S. Binkley, D. J. Defrees, J. Baker, J. P. Stewart, M. Head-Gordon, C. Gonzales, and J. A. Pople, GAUSSIAN 94, Revision B. 2./E.2., Gaussian, Inc., Pittsburgh, Pennsylvania, 1995.
[46] Extensible Computational Chemistry Environmental Basis Set Data Base, Version 10, 1996.
[47] S. F. Boys, and F. Bernardi, Mol. Phys. **19**, 553 (1970).
[48] V. Duijneveldt, in *Molecular Interactions*, edited by S. Scheiner (Wiley, New York, 1997), p. 81.
[49] J. Dyke, N. Jonathan, E. Lee, and A. Morris, J. Chem. Soc., Faraday Trans. 2 **72**, 1385 (1976).
[50] M. F. Jagod, C. M. Gabrys, M. Rosslein, D. Uy, and T. Oka, Can. J. Phys. **72**, 1192 (1994).
[51] W. P. Kraemer, and V. Spirko, J. Mol. Spectrosc. **149**, 235 (1991).
[52] P. Botschwina, in *Ion and Cluster Ion Spectroscopy and Structure*, edited by J. P. Maier (Elsevier, Amsterdam, 1989), p. 59.
[53] R. F. W. Bader, *Atoms in Molecules: A Quantum Theory* (Clarendon, Oxford, 1990).
[54] J. Cioslowski, P. J. Hay, and J. P. Ritchie, J. Phys. Chem. **94**, 148 (1990).
[55] Spectral line positions and detailed information about the *ab initio* potential energy surfaces are available upon request from dopfer@ubaclu.unibas.ch.
[56] A. J. Stone, *The Theory of Intermolecular Forces* (Clarendon, Oxford, 1996).
[57] G. Herzberg, *Molecular Spectra and Molecular Structure. II. Infrared and Raman Spectra of Polyatomic Molecules* (Krieger Publishing Company, Malabar, 1991).
[58] R. V. Olkhov, S. A. Nizkorodov, and O. Dopfer, J. Chem. Phys. **107**, 8229 (1997).
[59] D. J. Millen, Can. J. Chem. **63**, 1477 (1985).
[60] R. J. Le Roy, University of Waterloo Chemical Physics Report No. CP-555R, Level 6.1, 1996.
[61] E. P. L. Hunter and S. G. Lias, J. Phys. Chem. Ref. Data **27**, 413 (1998).
[62] O. Dopfer (unpublished results).
[63] W. T. Huntress, Astrophys. J., Suppl. **33**, 495 (1977).
[64] S. Davis, D. T. Anderson, G. Duxbury, and D. J. Nesbitt, J. Chem. Phys. **107**, 5661 (1997).
[65] J. K. Hovey and T. B. McMahon, J. Phys. Chem. **91**, 4560 (1987).